Upper-tropospheric inversion and easterly jet in the tropics

M. Fujiwara,[1] S.-P. Xie,[2] M. Shiotani,[3] H. Hashizume,[4] F. Hasebe,[1] H. Vömel,[5,6] S. J. Oltmans,[7] and T. Watanabe[8]

Received 28 June 2003; revised 25 August 2003; accepted 15 September 2003; published 31 December 2003.

[1] Shipboard radiosonde measurements revealed a persistent temperature inversion layer with a thickness of ~200 m at 12–13 km in a nonconvective region over the tropical eastern Pacific, along 2°N, in September 1999. Simultaneous relative humidity measurements indicated that the thin inversion layer was located at the top of a very wet layer with a thickness of 3–4 km, which was found to originate from the intertropical convergence zone (ITCZ) to the north. Radiative transfer calculations suggested that this upper tropospheric inversion (UTI) was produced and maintained by strong longwave cooling in this wet layer. A strong easterly jet stream was also observed at 12–13 km, centered around 4°–5°N. This easterly jet was in the thermal wind balance, with meridional temperature gradients produced by the cloud and radiative processes in the ITCZ and the wet outflow. Furthermore, the jet, in turn, acted to spread inversions further downstream through the transport of radiatively active water vapor. This feedback mechanism may explain the omnipresence of temperature inversions and layering structures in trace gases in the tropical troposphere. Examination of high-resolution radiosonde data at other sites in the tropical Pacific indicates that similar UTIs often appear around 12–15 km. The UTI around 12–15 km may thus be characterized as one of the ''climatological'' inversions in the tropical troposphere, forming the lower boundary of the so-called tropical tropopause layer, where the tropospheric air is processed photochemically and microphysically before entering the stratosphere. *INDEX TERMS:* 3374 Meteorology and Atmospheric Dynamics: Tropical meteorology; 3359 Meteorology and Atmospheric Dynamics: Radiative processes; 3314 Meteorology and Atmospheric Dynamics: Convective processes; 0368 Atmospheric Composition and Structure: Troposphere—constituent transport and chemistry; 0341 Atmospheric Composition and Structure: Middle atmosphere—constituent transport and chemistry (3334); *KEYWORDS:* easterly jet, temperature inversion, tropical upper troposphere

Citation: Fujiwara, M., S.-P. Xie, M. Shiotani, H. Hashizume, F. Hasebe, H. Vömel, S. J. Oltmans, and T. Watanabe, Upper-tropospheric inversion and easterly jet in the tropics, *J. Geophys. Res.*, *108*(D24), 4796, doi:10.1029/2003JD003928, 2003.

1. Introduction

[2] The tropical troposphere plays an important role in the general circulation and climate through latent heat release from deep convection and precipitation there. Several field campaigns have been made to characterize detailed structures of tropical convection, such as Global Atmospheric Research Program's Atlantic Tropical Experiment (GATE) in the Atlantic [e.g., *Houze and Betts*, 1981] and Tropical Ocean Global Atmosphere Coupled Ocean-Atmosphere Response Experiment (TOGA COARE) in the western Pacific [e.g., *Webster and Lukas*, 1992]. Tropical convective regions are often surrounded by extensive, clear-sky regions on synoptic to planetary scales [e.g., *Salby et al.*, 1991]. It has been pointed out that these clear-sky regions may also be important for Earth's energy balance because much of the Earth's radiation is emitted from the middle and upper tropospheric water vapor in these regions [e.g., *Pierrehumbert*, 1995; *Harries*, 1996]. Investigation of both convective and nonconvective regions is, therefore, needed for a better understanding of the tropical atmosphere.

[3] Radiosonde and ozonesonde soundings were made in September–October 1999 on board a research vessel, the *Shoyo-maru* of Japan Fisheries Agency, in the nonconvective, equatorial eastern Pacific region as well as in the

[1]Graduate School of Environmental Earth Science, Hokkaido University, Sapporo, Hokkaido, Japan.
[2]International Pacific Research Center and Department of Meteorology, University of Hawaii, Honolulu, Hawaii, USA.
[3]Radio Science Center for Space and Atmosphere, Kyoto University, Uji, Kyoto, Japan.
[4]Jet Propulsion Laboratory, Pasadena, California, USA.
[5]Cooperative Institute for Research in Environmental Sciences, University of Colorado, Boulder, Colorado, USA.
[6]Also at Climate Monitoring and Diagnostics Laboratory, National Oceanic and Atmospheric Administration, Boulder, Colorado, USA.
[7]Climate Monitoring and Diagnostics Laboratory, National Oceanic and Atmospheric Administration, Boulder, Colorado, USA.
[8]National Research Institute of Fisheries Science, Fisheries Research Agency, Yokohama, Kanagawa, Japan.

0148-0227/03/2003JD003928$09.00

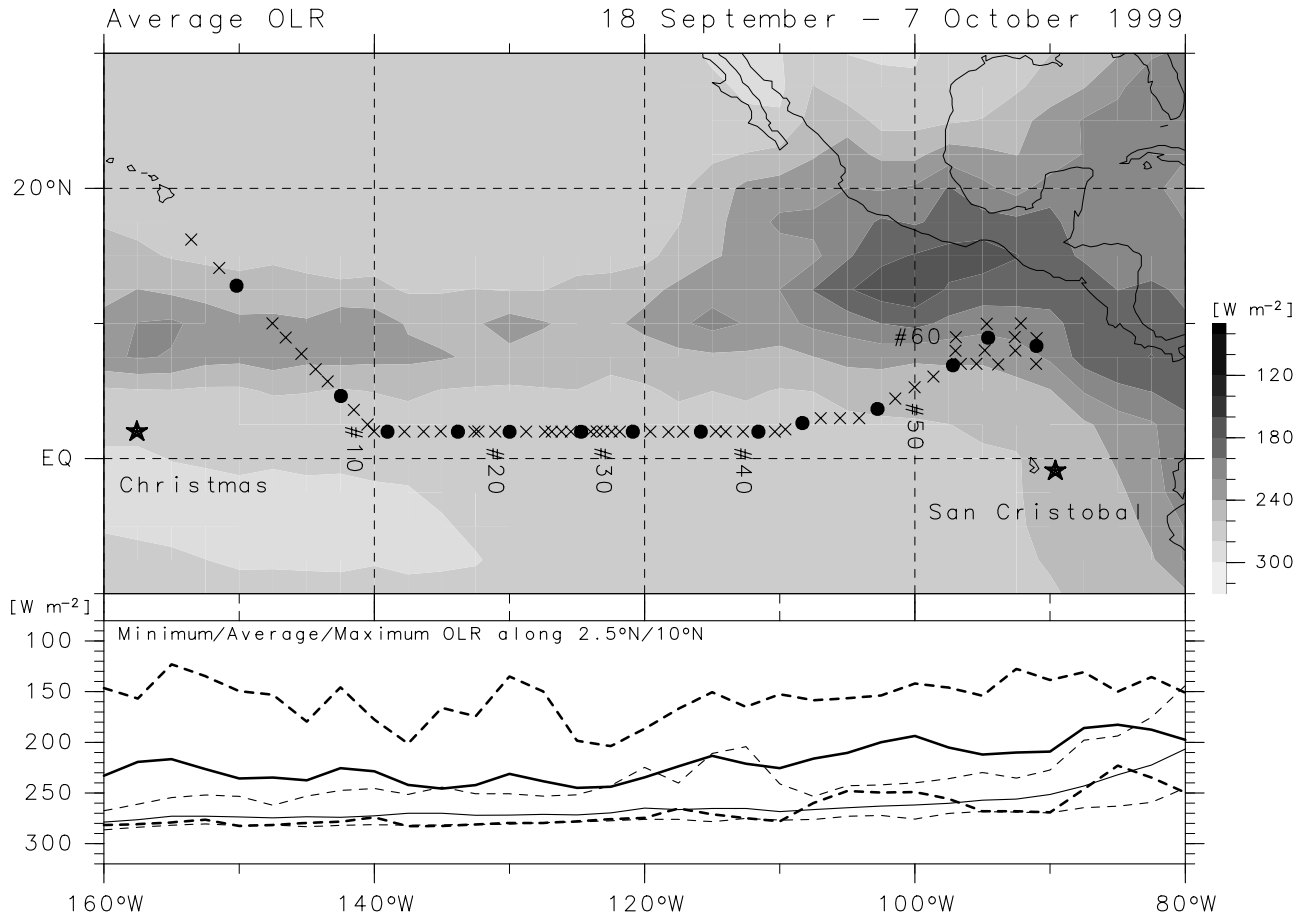

Figure 1. (top) Distribution of outgoing longwave radiation (OLR) averaged between 18 September and 7 October 1999, and (bottom) the average (solid line), and maximum and minimum (dashed lines) OLR along 2.5°N (thin line) and 10°N (bold line) during the same period. The daily interpolated OLR data is provided by the NOAA-CIRES Climate Diagnostics Center. Lower OLR values indicate higher cloud activity. The top panel also shows the locations of radiosonde (crosses) and ozonesonde (solid circles) soundings on the research vessel *Shoyo-maru*. The numbers denote the serial sounding number.

intertropical convergence zone (ITCZ) (Figure 1). The original purposes of the cruise were to investigate the atmospheric boundary layer response to slow sea surface temperature variations [*Hashizume et al.*, 2002] and to survey atmospheric ozone profiles across the equatorial eastern Pacific as a part of the Soundings of Ozone and Water in the Equatorial Region (SOWER) Pacific mission [*Shiotani et al.*, 2002]. Both are the first of their kinds in this region where few upper air soundings exist. During the cruise, a persistent, thin temperature inversion layer was observed at 12–13 km altitudes along 2°N (Figure 2). The inversion at such high altitudes is quite surprising because only patches of low-level stratocumulus and cumulus clouds were observed on the cruise along 2°N. The present paper aims at characterizing this upper tropospheric inversion layer (UTI) and the associated atmospheric conditions, discussing the mechanisms for its formation and maintenance based on the radiative heating rate calculations, and relating it to an easterly jet stream observed around the same altitudes.

[4] Inversion layers at and below ~5 km have already been reported in the tropics [e.g., *Hastenrath*, 1995; *Mapes and Zuidema*, 1996; *Johnson et al.*, 1996], and their possible interaction with convection, say, by enhancing detrainment, has been discussed. Atmospheric chemistry measurements on board aircrafts have also revealed the omnipresence of layering structures in water vapor, ozone, and other trace gases in the tropical lower and middle troposphere [e.g., *Danielsen et al.*, 1987; *Newell et al.*, 1999; *Stoller et al.*, 1999; see also *Shiotani et al.*, 2002], which probably have corresponding structures in thermal and dynamical properties. To our knowledge, inversion layers in the tropical upper troposphere have not been reported in the literature, but they may have important implications for the air transport across the tropical tropopause, a process key to the global stratospheric composition and climate [e.g., *Holton et al.*, 1995]. A recently proposed view on the tropical tropopause (16–18 km by traditional definitions) is that it should be regarded not as a surface but as a layer of a finite thickness, often called the tropical tropopause layer (TTL). The TTL's lower boundary is located typically around 13–15 km, above the influence of most convective transport and is defined by a lapse rate change or ozone vertical gradient change or zero clear-sky radiative heating rate or other equivalent criteria [e.g., *Folkins et*

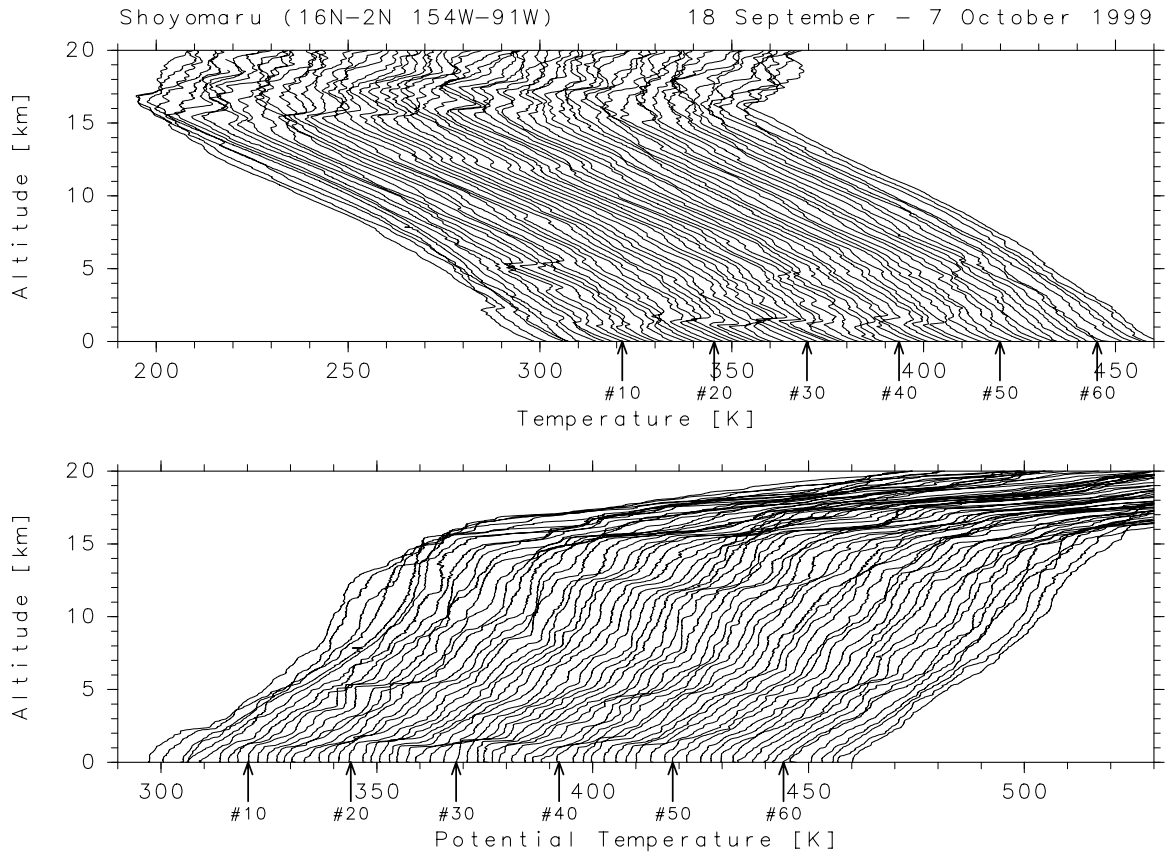

Figure 2. Vertical profiles of (top) temperature and (bottom) potential temperature observed, basically, every 6 hours (but sometimes every 3 or 12 hours) on the *Shoyo-maru* along the track shown in Figure 1. Successive profiles are displaced by 2.5 K. The sounding number is indicated for selected profiles by arrows at the surface (see also Figure 1).

al., 1999; *Gettelman and Forster*, 2002]. The tropospheric air is now considered to be processed photochemically and microphysically within the TTL before finally reaching the lower stratosphere. The transport across the bottom of the TTL is therefore an important factor for the troposphere-to-stratosphere transport. The UTI observed on the *Shoyo-maru* cruise can be regarded as the TTL's lower boundary in its extreme form. (Note that the longitudinal and seasonal variability in the altitude of the TTL's lower boundary has been suggested from ozone and water vapor observations [*Vömel et al.*, 2002; *Thompson et al.*, 2003].)

[5] Easterly jet streams are the prominent feature in the tropical upper troposphere, especially in the region from Southeast Asia across the tropical Indian Ocean and Africa to the tropical Atlantic, and are known to be in the thermal wind balance [e.g., *Koteswaram*, 1958; *Hastenrath*, 1995]. The easterly jet in the tropical eastern Pacific is much smaller in zonal extent and much shorter in time period, and thus has drawn less attention. Our analyses will reveal a close relationship between the easterly jet and the UTI in the tropical eastern Pacific.

[6] The rest of the paper is organized as follows. Section 2 describes the radiosonde and ozonesonde observation on the *Shoyo-maru* cruise. Section 3 analyzes the sounding data, presents the results of trajectory and radiation calculations, and discusses the mechanisms for the UTI and the easterly jet. Section 4 discusses the implications and summarizes the findings.

2. Observation

[7] Vertical profiles of pressure, temperature, relative humidity (RH), and horizontal wind velocity were measured with the Vaisala RS80-15G radiosondes equipped with the A-Humicap RH sensor. Vertical profiles of ozone were measured with the electrochemical concentration cell (ECC) ozonesondes flown with the RS80-15GE radiosondes. The sampling time interval of both sondes was 2 s. With the average ascending speed of $\sim$5 m s^{-1}, the vertical resolution of the data is $\sim$10 m. However, it should be noted that the sensor time lags for temperature, RH, and ozone are $<$2.5 s, 1 s at the surface (see http://www.vaisala.com), and typically $\sim$10 s, respectively. The RH sensor is known to have much slower time response in the upper troposphere [e.g., *Miloshevich et al.*, 2001].

[8] The RH measured with the Vaisala A-Humicap sensor is always reported with respect to liquid water as a convention. Hence the ice saturation below 0°C (above $\sim$5 km in the tropics) is less than 100%. See the saturation curves in the middle panels of Figure 6 (dashed) and in Figure 7a (thick dashed). *Fujiwara et al.* [2003] present the formula of

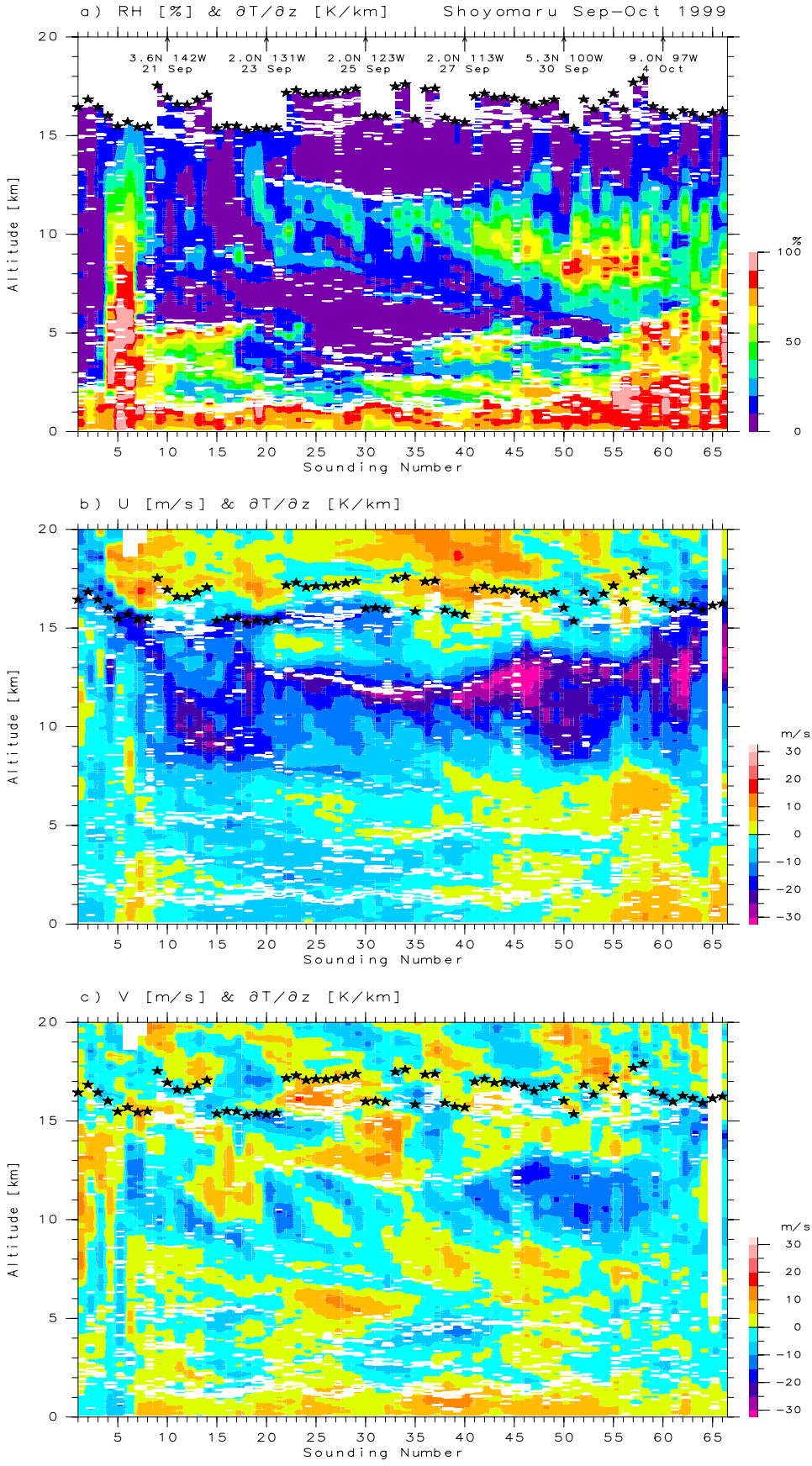
a) RH [%] & ∂T/∂z [K/km] Shoyomaru Sep–Oct 1999
3.6N 142W 21 Sep
2.0N 131W 23 Sep
2.0N 123W 25 Sep
2.0N 113W 27 Sep
5.3N 100W 30 Sep
9.0N 97W 4 Oct
Altitude [km]
Sounding Number
%
b) U [m/s] & ∂T/∂z [K/km]
m/s
c) V [m/s] & ∂T/∂z [K/km]
m/s

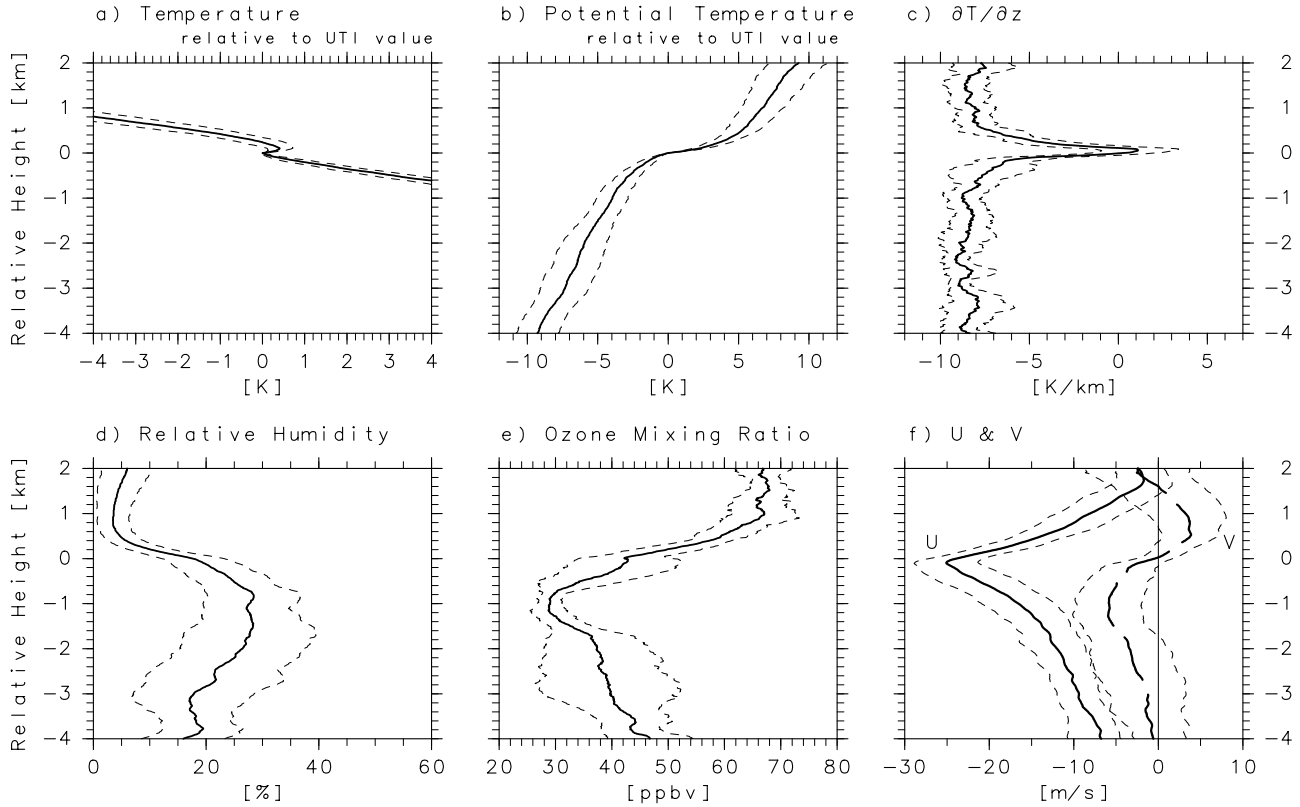

Figure 4. Composite profiles of (a) temperature, (b) potential temperature, (c) $\partial T/\partial z$, (d) RH (without correction), (e) ozone mixing ratio, and (f) zonal (solid lines) and meridional (broken lines) winds relative to the UTI altitude where temperature has a local minimum in each profile. Profiles for the sounding numbers 20 (2.0°N, 131°W, 23 September) to 41 (2.0°N, 112°W, 27 September) are used. Temperature and potential temperature are the ones relative to the average UTI values. Bold curves are the average, and the dashed curves show one standard deviation.

RH with respect to liquid water and ice saturation RH. Also, the A-Humicap sensor is known for its dry bias errors in the upper troposphere [e.g., *Miloshevich et al.*, 2001] and in the wet lower troposphere [*Fujiwara et al.*, 2003]. No correction is applied in Figures 3a and 4,, which should be regarded as a qualitative view. The so-called temperature-dependent correction for the middle to upper tropospheric measurements [*Miloshevich et al.*, 2001] is applied in Figure 6.

[9] Figure 1 shows the locations where radiosonde and ozonesonde soundings were conducted, superimposed on the distribution of outgoing longwave radiation (OLR) averaged between 18 September and 7 October 1999. The ITCZ is displaced to the north of the equator (around 10°N) in the eastern Pacific where cold sea water on and south of the equator prevents deep convection from occurring there [e.g., *Xie and Seki*, 1997]. Departing from Honolulu on 16 September 1999, the *Shoyo-maru* sailed southeastward and crossed the ITCZ at 10°N. Then it turned to the east, ran along 2°N where clear-sky conditions prevailed, and entered the ITCZ again east of 100°W. A total of 66 radiosondes and 14 ozonesondes were successfully launched during the cruise. The last sounding was made on 7 October 1999, and the leg ended at Manzanillo, Mexico, on 9 October 1999. Radiosonde soundings were conducted basically four times a day, with some exceptions (twice or eight times a day), while ozone soundings were made basically once daily. As the average speed of the ship near the equator was ~6 m s^{-1}, the profiles were obtained on average every 520 km for ozone and every 130 km for other parameters. See *Hashizume et al.* [2002] and *Shiotani et al.* [2002] for further details of the *Shoyo-maru* observation.

3. Results

3.1. Radiosonde Data Analysis

[10] Figure 2 shows successive vertical profiles of temperature and potential temperature observed on the *Shoyo-maru*. A persistent inversion layer, with a thickness of ~200 m and a temperature jump of ~0.5 K (see also Figure 4), is prominent around 12–13 km between the sounding number 20 and 41, between 130°W on

Figure 3. (opposite) Sounding number-altitude distributions of inversion layers (the regions with $\partial T/\partial z \geq 2$ K km^{-1} in the troposphere; white lines) and (a) RH (without correction), (b) zonal wind, and (c) meridional wind. RH above the cold-point tropopause (stars) are not shown. Positive values for winds correspond to westerly (eastward) and southerly (northward) in this paper. The location and date are indicated for selected soundings in Figure 3a.

23 September and 110°W on 27 September along 2°N (see Figure 1). This UTI is well distinguished from the strong inversion layers at the top of the marine boundary layer, the so-called trade(wind) inversions (see *Hashizume et al.* [2002] for details), and other inversions below 9 km including the so-called 0°C inversions at ~5 km [e.g., *Johnson et al.*, 1996], as well as from the cold-point tropopause above 15 km. The potential temperature jump for the UTI is typically 5 K, indicating that the UTI is a sharp boundary separating air masses above and below.

[11] Figure 3a shows the relationship between the RH distribution and the location of inversions. The UTI (around 12–13 km, the sounding numbers 20–41) is located at the top of a wet layer with a thickness of ~3–4 km. This wet layer was probably a water-vapor-rich layer or included some subvisible cirrus clouds (see section 3.3), whose origin will be discussed in section 3.2. Above the UTI, the air was extremely dry. The drop in RH across the UTI is greater than 50% after a correction is applied to the measured RH (see Figure 6). The UTI clearly corresponds to the bottom of the TTL where the tropospheric air is processed photochemically and microphysically before entering the stratosphere. Within the ITCZ (the sounding numbers ~5 or >41), we see only sporadic inversions in the upper troposphere. It should be noted that there is a common feature, a sharp humidity drop, at the trade inversions, inversions around 3 km, 0°C inversions, and the UTI around 12–13 km.

[12] Figures 3b and 3c show the zonal and meridional wind distributions in relation to inversion layers. A strong easterly jet is observed at the UTI and at 9–14 km for the sounding numbers >41 (2°–10°N). Note that Figure 3 can also be regarded as a meridional cross section for the sounding numbers >41 (see Figure 1). The center of the easterly jet, with a peak speed of >30 m s^{-1}, is located around 4°N at 12–13 km (180–160 hPa). As for the meridional wind, the UTI and the ~13 km level for the sounding numbers >41 correspond to a boundary between northerly (below) and southerly (above) wind regions.

[13] To better illustrate the vertical structure near the UTI, we composite the profiles of the sounding numbers 20–41 by placing the base of the UTI, the local temperature minimum at 11.8–12.8 km, at $z = 0$, where z is height. Figure 4 shows the composite profiles of temperature (T), potential temperature, $\partial T/\partial z$, RH, ozone mixing ratio, and horizontal winds. The temperature jump and the potential temperature jump for the UTI whose thickness is ~200 m are ~0.5 K and ~5 K, respectively. With the $\partial T/\partial z$ below and above the UTI being −8.5 K km^{-1}, the static stability ($\partial T/\partial z + g/c_p$, where g is gravitational acceleration, and c_p is specific heat of dry air at constant pressure [see, e.g., *Holton*, 1992]) in the UTI is about six times greater than in the background, inhibiting vertical mixing across the UTI. The UTI is indeed the boundary that separates distinct air masses below and above. The air mass below is wet with low ozone mixing ratios, while the one above is very dry with high ozone mixing ratios. The UTI is also a boundary that separates the northerly flow below from the southerly flow above. RH reaches a local maximum and ozone concentration a local minimum around 1 km below the UTI, indicating that the air mass originates from recent deep convection in the ITCZ and is advected southward. Indeed, the northerly flow peaks at the same altitude of the RH maximum and ozone minimum. We also see that the UTI corresponds to the center of an easterly jet. We will discuss this close relationship in section 3.4.

[14] Small-scale turbulence acts to mix air masses above and below the UTI and erode the UTI. The timescale for this erosion may be estimated as $(\Delta z)^2/(2K_z)$, where Δz is the layer thickness, and K_z is the vertical component of eddy diffusion coefficient [e.g., *Seinfeld and Pandis*, 1998, section 17]. If we take K_z as 2 m^2 s^{-1}, a lower limit around 10 km [*Fukao et al.*, 1994], the estimated timescale is 0.1 day for Δz = 200 m, and 3 days for Δz = 1 km. Therefore we need some mechanism to maintain the UTI that persisted for more than several days in our observation. This will be discussed in section 3.3.

3.2. Trajectory Analysis for the Wet Layer

[15] We investigate the origin of the wet layer at 10–12 km that is capped by the UTI using backward trajectory calculations. The trajectory model used here was developed at Earth Observation Research Center, National Space Development Agency of Japan. The European Centre for Medium-Range Weather Forecast (ECMWF) global operational analysis data was used as the input. Away from the ITCZ, air parcels nearly conserve their potential temperature, with trajectories roughly following isentropic surfaces. Figure 5 shows 3-day isentropic backward trajectories starting from the ozonesonde sounding points at 2°N at 11 km. It is seen that the wet layer has its origin in a convective region around 110°–90°W, 10°N. It is interesting to note that the *Shoyo-maru* ran nearly along some of the trajectories for the sounding numbers >13. Therefore, in Figure 3a, the wet layer below the UTI along 2°N (the sounding numbers 20–41) is a result of convective outflow from the similar altitude region with the sounding numbers >41.

3.3. Role of Radiation for the UTI

[16] This section examines the role of radiative cooling of the 10–12 km wet layer in the formation and maintenance of the UTI. Clear-sky radiative heating rate is calculated with a radiative transfer model based on the k distribution method with 13 bands (58 channels) in the shortwave and longwave radiation wavelengths [*Nakajima et al.*, 2000]. This model is incorporated in an atmospheric general circulation model developed at Center for Climate System Research and National Institute for Environmental Studies (CCSR/NIES) in Japan.

[17] *Shoyo-maru* soundings of temperature, pressure, and ozone were used from the sea surface to 30 km, and the U.S. Air Force Geophysics Laboratory (AFGL) tropical atmosphere model was used from 30 to 100 km. For water vapor, the sounding results were used up to ~14.5 km with the so-called temperature-dependent correction for the A-Humicap dry bias error presented by *Miloshevich et al.* [2001, equation (3)] between 0°C (~5 km) and −70°C (~14.5 km), and the AFGL model was applied for the above. The A-Humicap RH data may also suffer from another dry bias error in the lower troposphere, where (A-Humicap RH) $\simeq$ 0.9 × (true RH) for RH > 50% [*Fujiwara et al.*, 2003], but its impact on the radiation calculations in the upper troposphere is negligibly small for

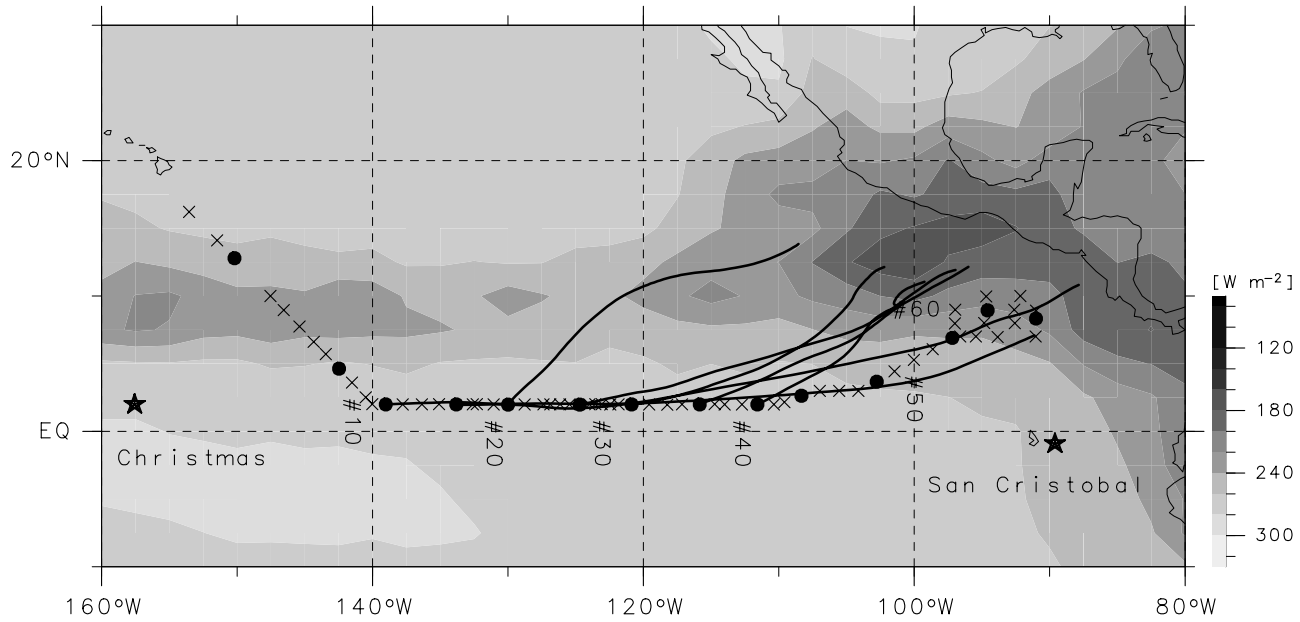

Figure 5. Three-day isentropic backward trajectories starting from the ozonesonde sounding points at 2°N (139°–112°W) at 11 km, superimposed on the top panel of Figure 1.

the present purpose. The concentrations of CO_2, CH_4, and N_2O from the AFGL model were also included in the calculation.

[18] Figure 6 shows the profiles of daily averaged heating rate as well as of temperature, ozone, and RH used in the calculation for the *Shoyo-maru* ozonesonde soundings on 24 (2.00°N, 124.86°W) and 26 (2.00°N, 115.97°W) September 1999. Note that after the correction, the wet layer at 10–12 km became nearly saturated with respect to ice. Although it cannot be ruled out that this wet layer included some optically thin cirrus clouds, here we assume a pure water vapor layer without cloud particles for simplicity. The estimated radiative cooling due to this wet layer may be considered as a lower limit because the presence of cirrus clouds would significantly increase the longwave cooling at their top [e.g., *Doherty et al.*, 1984]. Figure 6 clearly indicates a strong net cooling with ~3 K day^{-1} in the 10–12 km wet layer. This cooling comes exclusively from the water vapor rotation band (>10 μm), and the typical cooling rate under the average tropical conditions is ~1–2 K day^{-1} below 12 km and rapidly decreases to zero from 12 to 15 km [e.g., *Doherty and Newell*, 1984; *Doherty et al.*, 1984; *Folkins et al.*, 1999]. It should be noted that the lowest level of near-zero heating rate is located around 13 km, at the sharp drop in RH and at the UTI. Therefore, in this particular case, the TTL's lower boundary is located around 13 km.

[19] As a sensitivity test for the effect of the wet layer, Figure 7 shows radiative heating rate anomalies associated with a hypothetical layer of saturated water vapor placed at various altitudes. The top two panels show the reference for this test. It is well known that the longwave radiative cooling at wavelengths related to water vapor can be approximated by the "cooling-to-space" term [see *Rodgers and Walshaw*, 1966; *Mapes and Zuidema*, 1996], i.e., (cooling rate at height z) ≃ (Planck function at z) × (concentration of water vapor, a longwave emitter, at z) × (transmission between z and space). In the upper part of a wet layer, the factor of increasing water vapor concentration contributes to enhanced cooling anomalies. In the lower part of a wet layer, on the other hand, the factor of decreasing transmission to space reduces the cooling, and the trapping of longwave radiatic from the lower troposphere results in heating. Note that the sensitivities to the height and geometric thickness of the anomalous wet layer can be expressed in a function of optical thickness of the layer, which is proportional to the column integrated amount of water vapor in the layer. The nearly saturated wet layer at 10–12 km is found to be a strong (additional 1–4 K day^{-1}) and thick (>1 km) anamalous cooling layer.

[20] From these radiation calculations, it is suggested that the UTI was maintained and probably even produced by the strong radiative cooling associated with the wet layer located at 10–12 km which extended from the ITCZ (10°N, 110°–90°W) to the nonconvective region near the equator. This implicitly assumes that in this case, the radiative cooling was in part balanced by the temperature tendency term in the thermodynamic equation, not by the subsidence term only as is often assumed. (See, e.g., Chapter 11 of *Holton* [1992], and set the vertical scale smaller than the scale height H in the scale analysis of temperature (equation (11.9)).) In fact, Figure 3a shows that the wet layer does not descend as it moves southwestward along the air trajectories in Figure 5.

3.4. Easterly Jet and the UTI

[21] Figure 3b and Figure 4 also show a strong easterly jet at the UTI (for the sounding numbers 20–41) and at 9–14 km at 2°–10°N (for the sounding numbers >41). In this section, a unified view for the easterly jet and the UTI observed in the tropical eastern Pacific is explored in terms of the thermal wind balance.

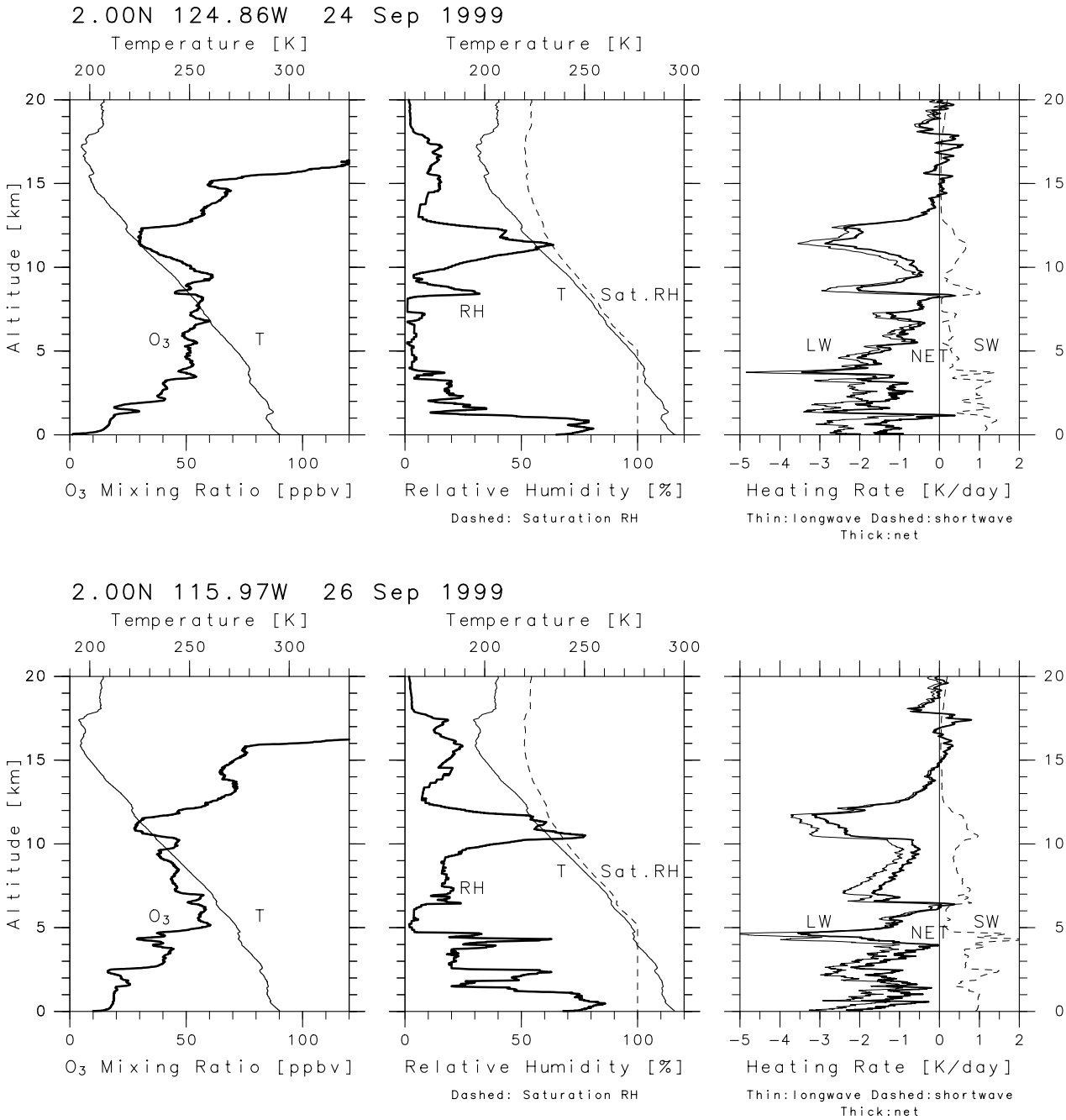

Figure 6. Vertical profiles of (left) ozone mixing ratio (bold lines) and temperature (thin lines), (middle) RH with respect to liquid water (bold solid lines), (ice-)saturation RH (dashed lines), and temperature (thin solid lines), and (right) daily averaged radiative heating rate (thick solid lines for net, thin solid lines for longwave, and dashed lines for shortwave) at (top) 2.00°N, 124.86°W on 24 September 1999 (the sounding number 27) and at (bottom) 2.00°N, 115.97°W on 26 September 1999 (the sounding number 37). The temperature-dependent correction has been applied to the measured RH. See text for details of the profiles used in the radiation calculations.

[22] The thermal wind equation, which comes from a combination of geostrophic wind equation and hydrostatic equation, is

$$\frac{\partial u}{\partial z} \simeq -\frac{g}{fT}\frac{\partial T}{\partial y}, \tag{1}$$

where u is eastward wind, f is the Coriolis parameter, and y is northward distance [e.g., *Andrews*, 2000]. On the equatorial β plane, where $\beta = df/dy$, equation (1) may become

$$\frac{\partial u}{\partial z} \simeq -\frac{g}{\beta T}\frac{\partial}{\partial y}\left(\frac{\partial T}{\partial y}\right) \tag{2}$$

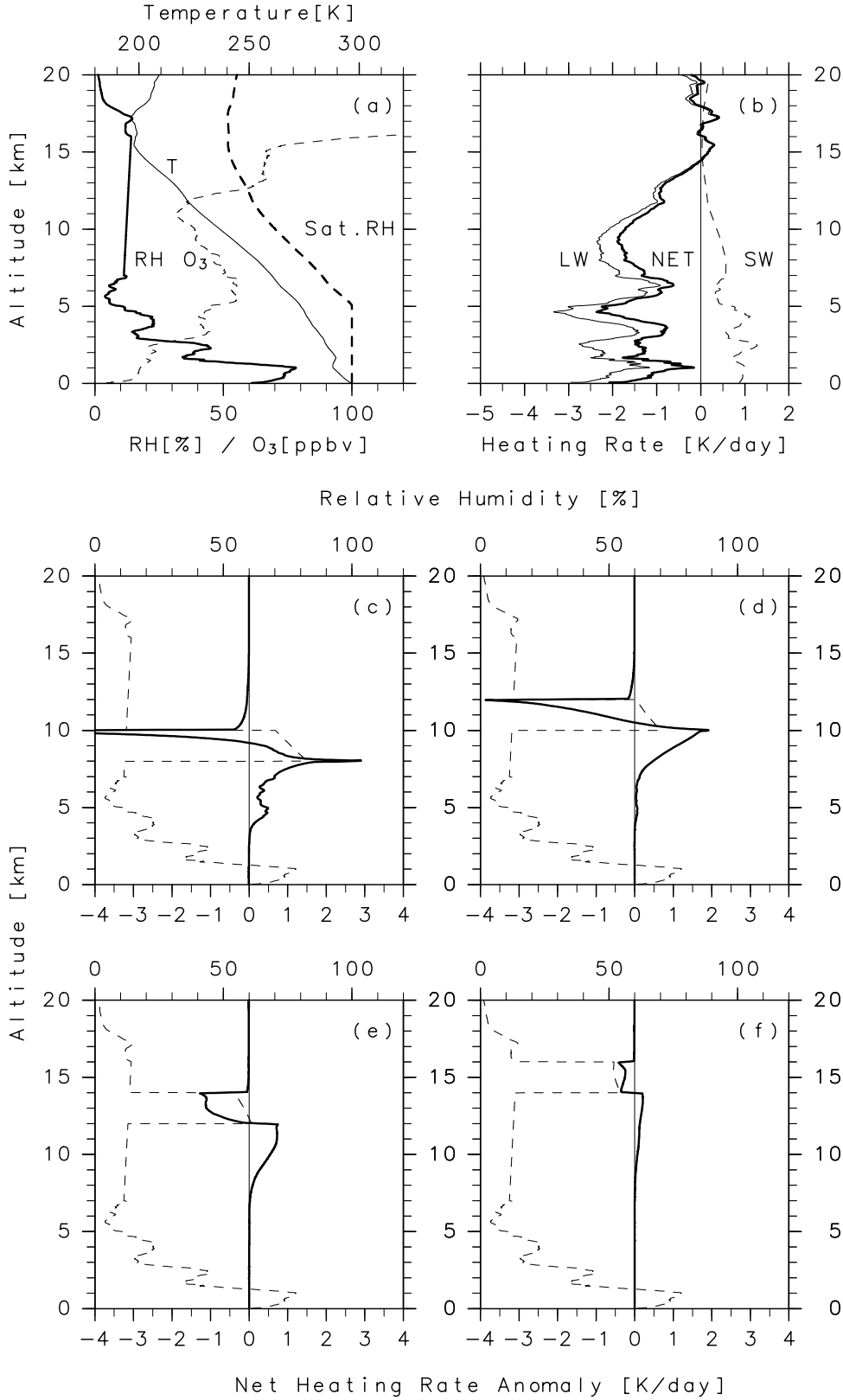

Figure 7. Sensitivity test for radiative heating anomalies due to a hypothetical, 2-km-thick saturated layer at different altitudes. (a and b) The reference profiles. The profiles in Figure 7a are obtained by averaging the profiles of the sounding numbers 20–41 for temperature (thin solid line), ozone (thin dashed line), saturation RH (bold dashed line), and RH (bold solid line), with RH from 7 to 16 km replaced by linearly interpolated values. Shown in Figure 7b are the radiative heating rate profiles (same as the right panels of Figure 6) calculated with the profiles in Figure 7a. The lower four panels show the net heating rate anomalies (solid lines) due to the saturated layers at (c) 8–10 km, (d) 10–12 km, (e) 12–14 km, and (f) 14–16 km, together with the RH profiles used (dashed lines).

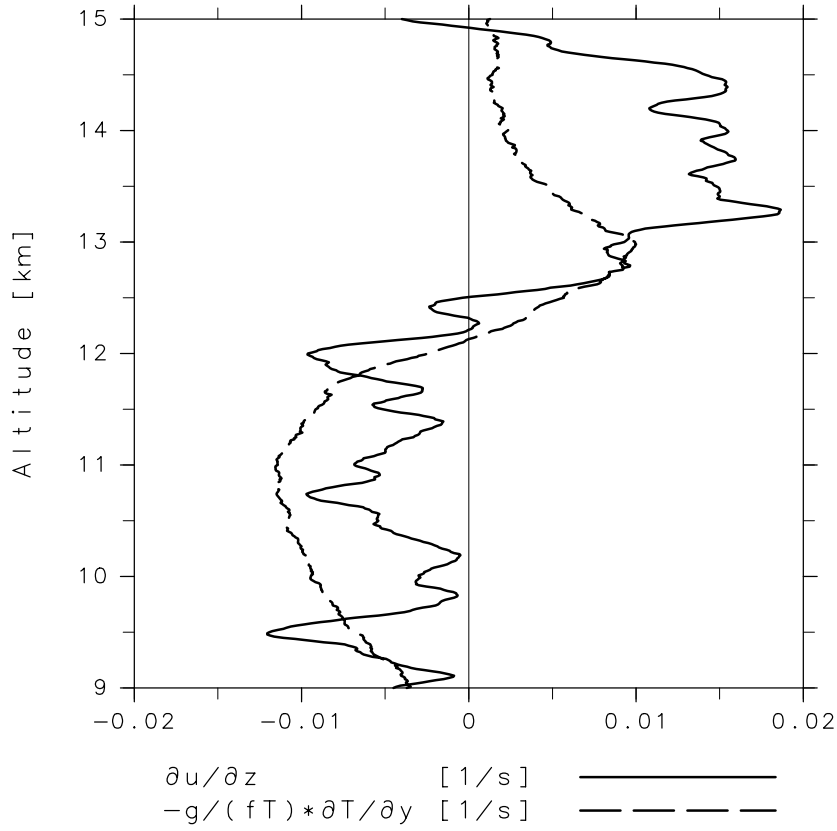

Figure 8. Profiles of zonal wind shear (solid line) averaged in 2.0°–5.3°N (the sounding numbers 42–50) and the right-hand side of equation (1) (dashed line). The term $\partial T/\partial y$ is calculated from the temperature difference between the sounding numbers 52–66 (7°–10°N) and the sounding numbers 20–41 (2°N) with a 6.5° latitude distance. The Coriolis parameter is set at its value at 4°N.

(see *Andrews et al.* [1987, section 8] for the derivation). Because the observed jet is located around 2°–10°N, we may need to consider equation (2) as well. Note the timescale to establish the geostrophic (hence thermal wind) balance is $1/|f|$ (e.g., ~1 day at 4°N) by considering the time for gravity waves to propagate over the Rossby's radius of deformation (see, for example, the discussion on the adjustment to geostrophic balance in a shallow-water system by *Holton* [1992]). Note also the factor $1/(fT)$ in equation (1). At lower latitudes in the upper troposphere, smaller meridional gradients of temperature can maintain the same zonal wind shear.

[23] Figure 8 shows the average zonal wind shear at 2.0°–5.3°N and the temperature difference between 7°–10°N and 2°N, the terms on the both sides of equation (1). From this figure, it is roughly confirmed that the observed easterly jet is in the thermal wind balance. The discrepancies may be due to the longitudinal shift of the *Shoyo-maru* track and/or due to the fact that in this case, equation (2) may be more suitable than equation (1).

[24] The ECMWF global operational analysis data is used to further investigate the relationship between the easterly jet and $\partial T/\partial y$ distributions. Comparison of the ECMWF data with the *Shoyo-maru* sounding data shows that the ECMWF data captures large-scale horizontal wind features including the center of the jet reasonably well, but does not resolve the very thin jet at the UTI and does not reproduce the dryness in the upper troposphere (not shown). Figure 9 shows the average zonal wind field at 200 hPa (~11.3 km) during the *Shoyo-maru* observation period. We see a localized easterly jet at 120°–90°W, equator to 10°N. The *Shoyo-maru* traced the southern and southeastern portions of the jet core, and the jet observed at the UTI on the *Shoyo-maru* is the southwestern portion of the jet. Figure 10 shows the latitude-altitude distributions of u and $\partial T/\partial y$ averaged at 110°–100°W during the same period. We see a negative $\partial T/\partial y$ in the westerly shear region above the tropical jet core and a positive $\partial T/\partial y$ in the easterly shear region below the jet core. However, we may notice in Figure 10 that the jet axis is rather tilted and located at slightly lower latitudes. The latter may be explained by equation (2). When the equatorial β plane approximation is more suitable, the jet axis should be located at the lower-latitude edge of the axis of the maximum and minimum $\partial T/\partial y$.

[25] The easterly jet displays pronounced temporal variability. Figure 11 shows the longitude-time sections of ECMWF zonal and meridional winds at 200 hPa at 5°N and of OLR at 10°N. The speed of the easterly jet at 140°–90°W fluctuates at a timescale of about half a month, with coherent variations in the northerly wind and cloud activity in the ITCZ. Note that even during the periods when the jet is weaker in Figure 11, the same relationship between u and $\partial T/\partial y$ as in Figure 10 holds (not shown).

[26] On the basis of the above analyses we propose the following scenario for the structure of the upper troposphere including the UTI and the easterly jet (Figure 12). The

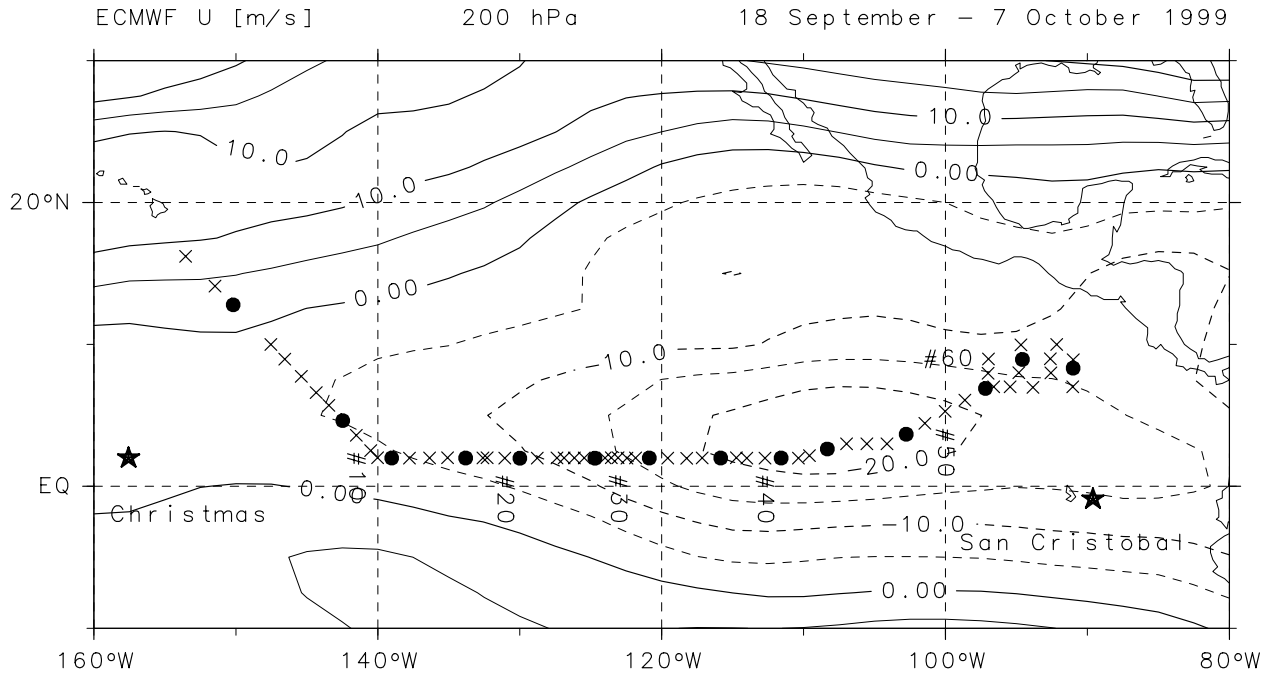

Figure 9. ECMWF zonal wind distribution at 200 hPa (~11.3 km) averaged between 18 September and 7 October 1999. Contour interval is 5 m s^{-1}, and negative contours (easterly) are dashed. Sounding locations are also shown.

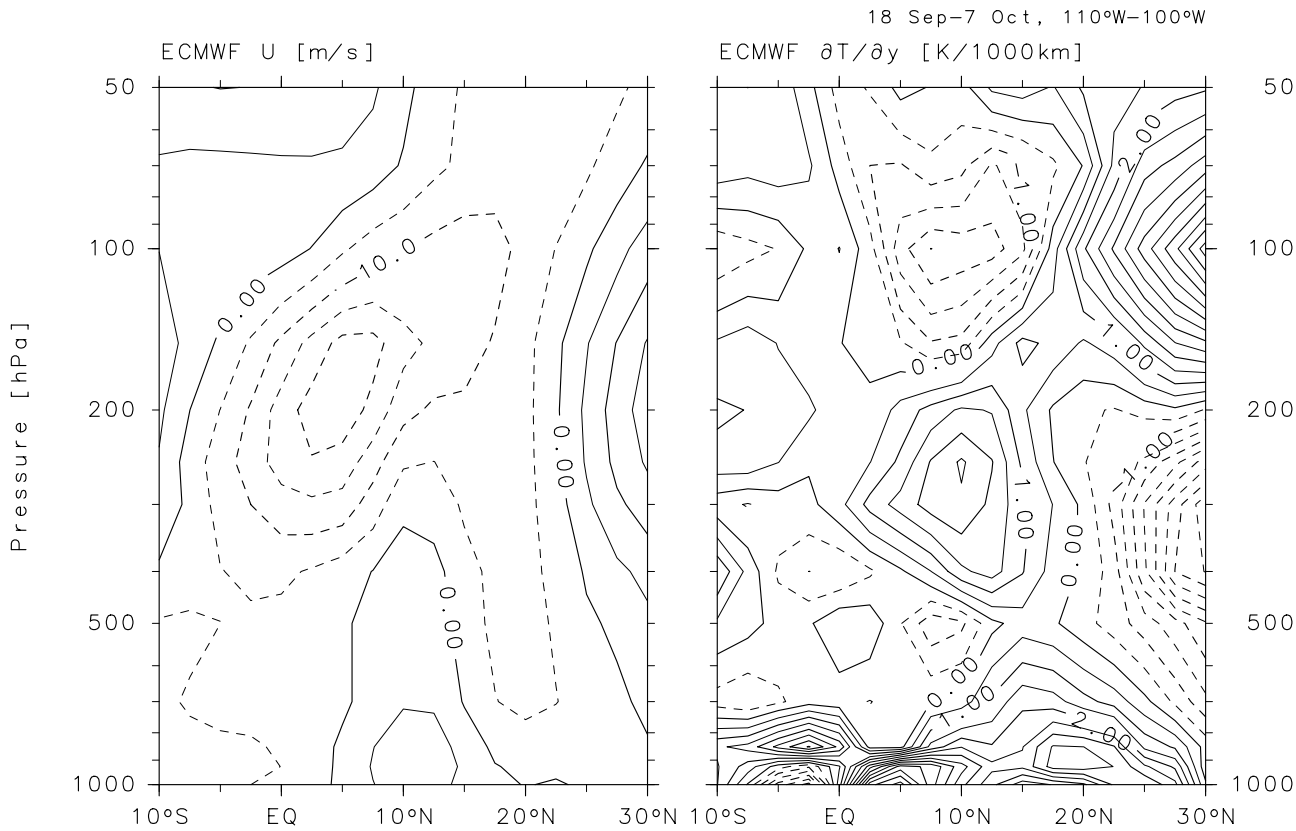

Figure 10. Latitude-pressure (altitude) distributions of (left) ECMWF zonal wind and (right) ECMWF meridional gradient of temperature, averaged at 110°–100°W between 18 September and 7 October 1999. Pressures, 500 hPa, 200 hPa, and 100 hPa correspond to 4.9 km, 11.3 km, and 16.1 km, respectively. Contour intervals are 5 m s^{-1} for the left panel and 0.5 K $(1000\ km)^{-1}$ for the right panel. Negative contours are dashed.

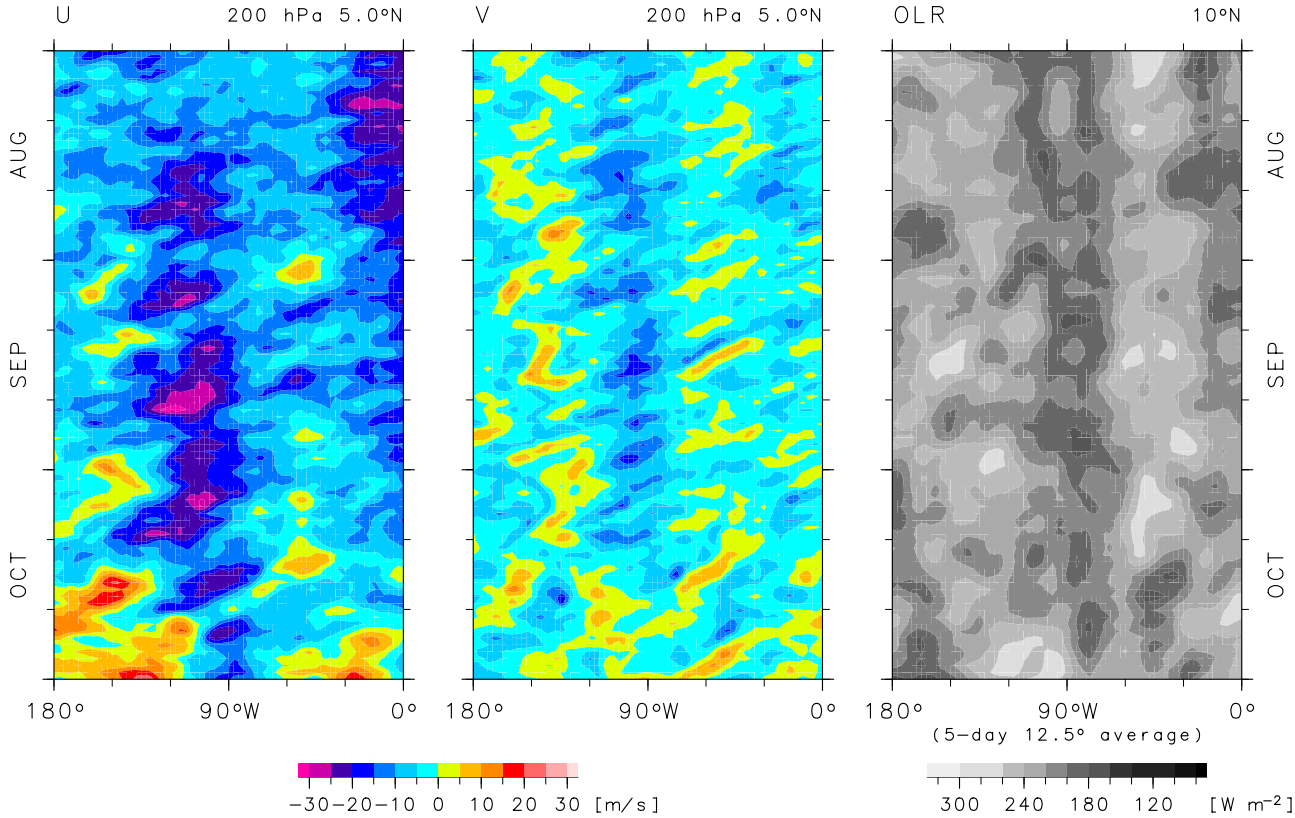

Figure 11. Longitude-time distributions of (left) ECMWF zonal wind and (center) ECMWF meridional wind at 200 hPa at 5°N and (right) OLR at 10°N. OLR data are running averaged for 5 days and 12.5° longitude.

southward transport of wet air at 10–12 km from deep convection in the ITCZ causes a strong radiative cooling anomaly around 12–13 km, producing the UTI near the equator. Below 12–13 km, $\partial T/\partial y$ is positive between this cold anomaly and the warm air at the same altitudes over the ITCZ region due to latent heat release. Above 12–13 km, on the other hand, $\partial T/\partial y$ is negative because the region over the ITCZ convection is cooled by a deficit of longwave radiation from the lower troposphere. The resultant, meridional cold and warm anomaly pattern is balanced with the easterly jet centered at 12–13 km, in 4°–5°N and 120°–90°W. The important controlling factor of this system is the convection in the ITCZ.

[27] The easterly jet then transports the wet air further to the west, during which the radiative cooling continues to operate. This is probably the principal mechanism for the large zonal extent of the UTI observed on the *Shoyo-maru* cruise.

[28] The strength of easterly jet displays significant variability (Figure 11), which might result from the variability in the strength of ITCZ convection and hence the strength of its outflow in the upper troposphere. Finally, we note that meridional winds reverse their direction at the UTI, being southerly above in the TTL and northerly below (Figures 3c and 4f). The dynamics of the southerly winds above the UTI in the TTL is not clear at this moment.

4. Discussion and Conclusions

[29] An inversion layer with a wet air mass below and a dry air mass above is radiatively and dynamically a stable system. The strong net radiative cooling by water vapor in the upper part of the wet region acts to strengthen the inversion layer above [e.g., *Mapes and Zuidema*, 1996], preventing air masses above and below from turbulent mixing. In the convective region, strong convection removes weak inversion layers. Such inversions, on the other hand, may force moderate convection to detrain mass and prevent it from further development. The wet outflow extending horizontally from the convective to nonconvec-

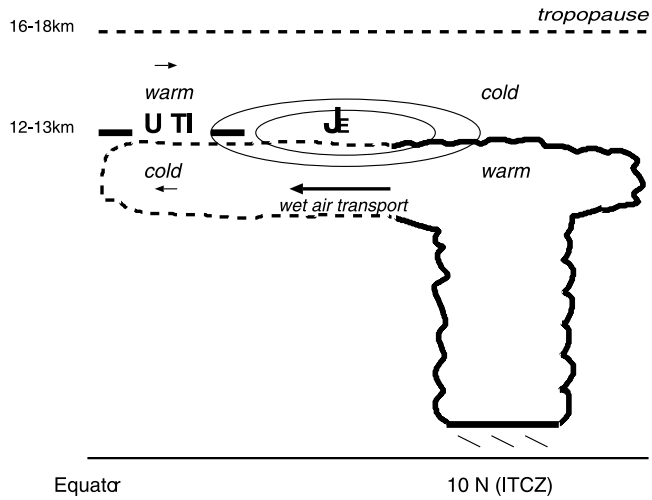

Figure 12. Schematic illustration of the observed system including the UTI and the easterly jet. See text for details.

tive regions strengthens preexisting inversions and/or establishes new inversions through the water vapor radiation effect (see other examples in Figure 3a, e.g., the sounding numbers 5–20 and around 5 km). This study shows that the water vapor radiation effect is responsible for the UTI, a high-altitude inversion layer that had not been reported previously. We further suggest that the regional-scale inversions, with horizontal temperature gradients, are involved in maintaining an easterly jet that transports water vapor and other trace gases further downstream. This feedback mechanism between the transport of radiatively active water vapor and the formation of a jet through the thermal wind relationship may explain the omnipresence of inversion layers and layering structures in trace gases in the tropical troposphere.

[30] The UTI seems a common feature of the tropical upper troposphere that had been overlooked. During the *Shoyo-maru* observation period, persistent UTIs were also observed in concurring soundings at San Cristóbal Island (0.9°S, 89.6°W) in the Galápagos Islands (two cases) and at Christmas Island (1.52°N, 157.20°W), Kiribati, as part of the SOWER campaign (see Figure 1). These UTIs had the life time of 9–12 days at San Cristóbal and 3 days at Christmas Island, all showing a descending trend in time from 15 to 12.5 or 13 km. The equatorial Kelvin waves may cause this descent as in a case at San Cristóbal in September 1998 [*Fujiwara et al.*, 2001]. Persistent UTIs were also observed in soundings near or at Kototabang (0.20°S, 100.3°E), Indonesia in December 2000 (T. Horinouchi, personal communication, 2002) and in August 2001 (N. Okamoto, personal communication, 2002). These UTIs persisted for 10–15 days, both showing an ascending trend from 14 to 15.5–16 km. The vertical sampling interval of 10–50 m is essential to capture these UTIs.

[31] The UTI described here does not occur randomly in height. Instead, it favors an altitude range of 12–15 km and always forms below the TTL. Thus the UTI around 12–15 km may be characterized as one of the ''climatological'' inversions in that it occurs frequently and forms by well-defined mechanisms, such as the trade inversions and the 0°C inversions. Furthermore, the UTI may form the lower boundary of the TTL, a hypothesis supported by the following observations: the UTI observed on the *Shoyo-maru* cruise is located at the top of a wet outflow from the deep convection in the ITCZ (Figures 3a and 5); net radiative heating rate rapidly approaches zero above the UTI (Figure 6); and the UTI separates wet and ozone-poor air mass below and dry and ozone-rich air mass above (Figure 4). It should be noted that previous works [e.g., *Folkins et al.*, 1999] reported the level of zero net heating rate around 15 km because they use averaged profiles of water vapor, not high-resolution sounding data that often contain sharp changes in water vapor. The strong stratification at the UTI (Figure 4c) strongly limits air exchange and should be taken into account for the troposphere-to-stratosphere air transport. Further studies are necessary to confirm this proposed UTI-TTL relationship.

[32] **Acknowledgments.** We are deeply obliged to Japan Fisheries Agency for providing us the shiptime on the *Shoyo-maru* and to Captain K. Kubota, K. Oshima, S. Sawadaishi, and the *Shoyo-maru* crew for their extensive collaboration. This work was supported in part by the International Scientific Research Program and the Grant-in-aid for Scientific Research of Priority Areas (B), No. 11219202, MEXT, by Frontier Research System for Global Change, and by NASA. M.F. was supported by research fellowships of the Japan Society for the Promotion of Science for Young Scientists. Comments on the manuscript by reviewers were appreciated. Figures (except Figure 12) were produced with the GFD-DENNOU Library. IPRC contribution 236 and SOEST contribution 6257.

References

Andrews, D. G., *An Introduction to Atmospheric Physics*, 229 pp., Cambridge Univ. Press, New York, 2000.

Andrews, D. G., J. R. Holton, and C. B. Leovy, *Middle Atmosphere Dynamics*, 489 pp., Academic, San Diego, Calif., 1987.

Danielsen, E. F., S. E. Gaines, R. S. Hipskind, G. L. Gregory, G. W. Sachse, and G. F. Hill, Meteorological context for fall experiments including distributions of water vapor, ozone, and carbon monoxide, *J. Geophys. Res.*, *92*, 1986–1994, 1987.

Doherty, G. M., and R. E. Newell, Radiative effects of changing atmospheric water vapour, *Tellus, Ser. B*, *36*, 149–162, 1984.

Doherty, G. M., R. E. Newell, and E. F. Danielsen, Radiative heating rates near the stratospheric fountain, *J. Geophys. Res.*, *89*, 1380–1384, 1984.

Folkins, I., M. Loewenstein, J. Podolske, S. J. Oltmans, and M. Proffitt, A barrier to vertical mixing at 14 km in the tropics: Evidence from ozonesondes and aircraft measurements, *J. Geophys. Res.*, *104*, 22,095–22,102, 1999.

Fujiwara, M., F. Hasebe, M. Shiotani, N. Nishi, H. Vömel, and S. J. Oltmans, Water vapor control at the tropopause by equatorial Kelvin waves observed over the Galápagos, *Geophys. Res. Lett.*, *28*, 3143–3146, 2001.

Fujiwara, M., M. Shiotani, F. Hasebe, H. Vömel, S. J. Oltmans, P. W. Ruppert, T. Horinouchi, and T. Tsuda, Performance of the Meteolabor ''Snow White'' chilled-mirror hygrometer in the tropical troposphere: Comparisons with the Vaisala RS80 A/H-Humicap sensors, *J. Atmos. Oceanic Technol.*, *20*, 1534–1542, 2003.

Fukao, S., M. D. Yamanaka, N. Ao, W. K. Hocking, T. Sato, M. Yamamoto, T. Nakamura, T. Tsuda, and S. Kato, Seasonal variability of vertical eddy diffusivity in the middle atmosphere: 1. Three-year observations by the middle and upper atmosphere radar, *J. Geophys. Res.*, *99*, 18,973–18,987, 1994.

Gettelman, A., and P. M. de F. Forster, A climatology of the tropical tropopause layer, *J. Meteorol. Soc. Jpn.*, *80*(4B), 911–924, 2002.

Harries, J. E., The greenhouse Earth: A view from space, *Q. J. R. Meteorol. Soc.*, *122*, 799–818, 1996.

Hashizume, H., S.-P. Xie, M. Fujiwara, M. Shiotani, T. Watanabe, Y. Tanimoto, W. T. Liu, and K. Takeuchi, Direct observations of atmospheric boundary layer response to SST variations associated with tropical instability waves over the eastern equatorial Pacific, *J. Clim.*, *15*, 3379–3393, 2002.

Hastenrath, S., *Climate Dynamics of the Tropics*, 488 pp., Kluwer Acad., Norwell, Mass., 1995.

Holton, J. R., *An Introduction to Dynamic Meteorology*, 3rd ed., 511 pp., Academic, San Diego, Calif., 1992.

Holton, J. R., P. H. Haynes, M. E. McIntyre, A. R. Douglass, R. B. Rood, and L. Pfister, Stratosphere-troposphere exchange, *Rev. Geophys*, *33*, 403–439, 1995.

Houze, R. A., Jr., and A. K. Betts, Convection in GATE, *Rev. Geophys.*, *19*, 541–576, 1981.

Johnson, R. H., P. E. Ciesielski, and K. A. Hart, Tropical inversions near the 0°C level, *J. Atmos. Sci.*, *53*, 1838–1855, 1996.

Koteswaram, P., The easterly jet stream in the tropics, *Tellus*, *10*, 43–57, 1958.

Mapes, B. E., and P. Zuidema, Radiative-dynamical consequences of dry tongues in the tropical troposphere, *J. Atmos. Sci.*, *53*, 620–638, 1996.

Miloshevich, L. M., H. Vömel, A. Paukkunen, A. J. Heymsfield, and S. J. Oltmans, Characterization and correction of relative humidity measurements from Vaisala RS80-A radiosondes at cold temperatures, *J. Atmos. Oceanic Technol.*, *18*, 135–156, 2001.

Nakajima, T., M. Tsukamoto, Y. Tsushima, A. Numaguti, and T. Kimura, Modeling of the radiative process in an atmospheric general circulation model, *Appl. Opt.*, *39*, 4869–4878, 2000.

Newell, R. E., V. Thouret, J. Y. N. Cho, P. Stoller, A. Marenco, and H. G. Smit, Ubiquity of quasi-horizontal layers in the troposphere, *Nature*, *398*, 316–319, 1999.

Pierrehumbert, R. T., Thermostats, radiator fins, and the local runaway greenhouse, *J. Atmos. Sci.*, *52*, 1784–1806, 1995.

Rodgers, C. D., and C. D. Walshaw, The computation of infra-red cooling rate in planetary atmospheres, *Q. J. R. Meteorol. Soc.*, *92*, 67–92, 1966.

Salby, M. L., H. H. Hendon, K. Woodberry, and K. Tanaka, Analysis of global cloud imagery from multiple satellites, *Bull. Am. Meteorol. Soc.*, *72*, 467–480, 1991.

Seinfeld, J. H., and S. N. Pandis, *Atmospheric Chemistry and Physics: From Air Pollution to Climate Change*, 1326 pp., Wiley-Interscience, Hoboken, N. J., 1998.

Shiotani, M., M. Fujiwara, F. Hasebe, H. Hashizume, H. Vömel, S. J. Oltmans, and T. Watanabe, Ozonesonde observations in the equatorial Eastern Pacific—The Shoyo-maru survey, *J. Meteorol. Soc. Jpn.*, *80*(4B), 897–909, 2002.

Stoller, P., et al., Measurements of atmospheric layers from the NASA DC-8 and P-3B aircraft during PEM-Tropics A, *J. Geophys. Res.*, *104*, 5745–5764, 1999.

Thompson, A. M., et al., Southern Hemisphere Additional Ozonesondes (SHADOZ) 1998–2000 tropical ozone climatology: 2. Tropospheric variability and the zonal wave-one, *J. Geophys. Res.*, *108*(D2), 8241, doi:10.1029/2002JD002241, 2003.

Vömel, H., S. J. Oltmans, B. J. Johnson, F. Hasebe, M. Shiotani, M. Fujiwara, N. Nishi, M. Agama, J. Cornejo, F. Paredes, and H. Enriquez, Balloon-borne observations of water vapor and ozone in the tropical upper troposphere and lower stratosphere, *J. Geophys. Res.*, *107*(D14), 4210, doi:10.1029/2001JD000707, 2002.

Webster, P. J., and R. Lukas, TOGA COARE: The coupled ocean-atmosphere response experiment, *Bull. Am. Meteorol. Soc.*, *73*, 1377–1416, 1992.

Xie, S.-P., and M. Seki, Causes of equatorial asymmetry in sea surface temperature over the eastern Pacific, *Geophys. Res. Lett.*, *24*, 2581–2584, 1997.

M. Fujiwara and F. Hasebe, Graduate School of Environmental Earth Science, Hokkaido University, Sapporo, Hokkaido 060-0810, Japan. (fuji@ees.hokudai.ac.jp)

H. Hashizume, Jet Propulsion Laboratory, Pasadena, CA 91109-8099, USA.

S. J. Oltmans, Climate Monitoring and Diagnostics Laboratory, National Oceanic and Atmospheric Administration, Boulder, CO 80305, USA.

M. Shiotani, Radio Science Center for Space and Atmosphere, Kyoto University, Uji, Kyoto 611-0011, Japan.

H. Vömel, Cooperative Institute for Research in Environmental Sciences, University of Colorado, Boulder, CO 80309-0216, USA.

T. Watanabe, National Research Institute of Fisheries Science, Fisheries Research Agency, Yokohama, Kanagawa 236-8648, Japan.

S.-P. Xie, International Pacific Research Center and Department of Meteorology, University of Hawaii, Honolulu, HI 96822, USA.